membranes

MDPI

Article

Cationic Imidazolium-Urethane-Based Poly(Ionic Liquids) Membranes for Enhanced CO_2/CH_4 Separation: Synthesis, Characterization, and Performance Evaluation

Guilherme Dias [1,2], Laura Rocca [1], Henrique Z. Ferrari [1,2], Franciele L. Bernard [1], Fernando G. Brandão [3], Leonardo Pereira [3] and Sandra Einloft [1,*]

[1] School of Technology, Pontifical Catholic University of Rio Grande do Sul (PUCRS), Porto Alegre 90619-900, RS, Brazil; guilherme.dias@acad.pucrs.br (G.D.); l.rocca@edu.pucrs.br (L.R.); henrique.zucchetti@edu.pucrs.br (H.Z.F.); franciele.bernard@pucrs.br (F.L.B.)

[2] Post-Graduation Program in Materials Engineering and Technology, Pontifical Catholic University of Rio Grande do Sul (PUCRS), Porto Alegre 90619-900, RS, Brazil

[3] Petrobras/CENPES, Ilha do Fundão Qd. 07, Rio de Janeiro 21941-915, RJ, Brazil; fernando.brandao@petrobras.com.br (F.G.B.); lspereira@petrobras.com.br (L.P.)

* Correspondence: einloft@pucrs.br

Abstract: The escalating emissions of CO_2 into the atmosphere require the urgent development of technologies aimed at mitigating environmental impacts. Among these, aqueous amine solutions and polymeric membranes, such as cellulose acetate and polyimide are commercial technologies requiring improvement or substitution to enhance the economic and energetic efficiency of CO_2 separation processes. Ionic liquids and poly(ionic liquids) (PILs) are candidates to replace conventional CO_2 separation technologies. PILs are a class of materials capable of combining the favorable gas affinity exhibited by ionic liquids (ILs) with the processability inherent in polymeric materials. In this context, the synthesis of the IL GLYMIM[Cl] was performed, followed by ion exchange processes to achieve GLYMIM variants with diverse counter anions (NTf_2^-, PF_6^-, and BF_4). Subsequently, PIL membranes were fabricated from these tailored ILs and subjected to characterization, employing techniques such as SEC, FTIR, DSC, TGA, DMA, FEG-SEM, and CO_2 sorption analysis using the pressure decay method. Furthermore, permeability and ideal selectivity assessments of CO_2/CH_4 mixture were performed to derive the diffusion and solubility coefficients for both CO_2 and CH_4. PIL membranes exhibited adequate thermal and mechanical properties. The PIL-BF_4 demonstrated CO_2 sorption capacities of 33.5 mg CO_2/g at 1 bar and 104.8 mg CO_2/g at 10 bar. Furthermore, the PIL-BF_4 membrane exhibited permeability and ideal (CO_2/CH_4) selectivity values of 41 barrer and 44, respectively, surpassing those of a commercial cellulose acetate membrane as reported in the existing literature. This study underscores the potential of PIL-based membranes as promising candidates for enhanced CO_2 capture technologies.

Keywords: CO_2 capture; poly(ionic liquids); ionic liquids; polyurethane; permeability

check for updates

Citation: Dias, G.; Rocca, L.; Ferrari, H.Z.; Bernard, F.L.; Brandão, F.G.; Pereira, L.; Einloft, S. Cationic Imidazolium-Urethane-Based Poly(Ionic Liquids) Membranes for Enhanced CO_2/CH_4 Separation: Synthesis, Characterization, and Performance Evaluation. *Membranes* **2024**, *14*, 151. https://doi.org/10.3390/membranes14070151

Academic Editors: Naiying Du and Haiqing Lin

Received: 31 May 2024
Revised: 2 July 2024
Accepted: 4 July 2024
Published: 9 July 2024

1. Introduction

In the context of contemporary technological progress, a noticeable increase in atmospheric CO_2 emissions originating from the utilization of fossil resources has emerged [1,2]. In response, the imperative to develop new technologies or refine existing ones to improve environmental impacts has become increasingly evident. A particularly promising avenue of investigation lies in CO_2 capture. This technological approach garners attention due to its applicability to major emission sources and its potential for the recovery and repurposing of CO_2 for other industrial processes [2,3]. Currently, diverse techniques for CO_2 capture exists, among which amine solutions and polymeric membranes stand out as exemplary materials employed for this purpose [4]. The amine-based capture method, which involves

the chemical absorption of CO_2, is widely used in emission plants for handling combustion gases and in natural gas sweetening [5–9]. Despite its cost effectiveness, this approach presents challenges such as the generation of undesirable by-products, the formation of corrosive acids leading to the degradation of the internals of the reactor, volatility, and the high energy costs associated with CO_2 recovery, thus diminishing its attractiveness over time [10]. On the other hand, the utilization of membranes in CO_2 separation demonstrates significant potential due to their adaptability to high CO_2 concentrations and their more compact structural requirements compared to amine solutions [11]. Ionic liquids (ILs) constitute a class of organic salts composed of a cation and an anion, being an organic cation and an organic or inorganic anion [4,12–14]. Characterized by a melting temperature below 100 °C, ILs possess several properties expected of effective CO_2 capture materials, including low vapor pressure, non-flammability, thermal stability, low corrosiveness, minimal decomposition rates, lower recovery costs, and environmental compatibility vis-à-vis organic solvents [4,12,15,16]. ILs have attracted attention in the domain of combustion gas capture due to their enhanced CO_2 affinity relative to gas mixtures containing N_2 and CH_4. However, ILs present specific attributes that impede their immediate adoption in CO_2 capture plants, such as high production costs and complexity compared to amine solutions, as well as high viscosity resulting in suboptimal CO_2 sorption/desorption rates [4]. Polymerized ionic liquids or poly(ionic liquids) (PILs) represent a distinct class of materials with broad applicability across various scientific domains [17–21]. Typically composed of a polymeric structure hosting an ionic liquid unit for each polymer repeat unit, PILs offer superior CO_2 sorption/desorption kinetics, thus conferring a significant advantage over ILs [12,22–25]. Condensation polymerization stands out as a common method for PIL synthesis. Researchers, including Bernard 2019, da Luz 2021, and Morozova 2020 [26–28] have successfully synthesized PILs and assessed their properties. Materials such as PTMG (polytetramethylene glycol), PCD (polycarbonate diol), and PCL (polycaprolactone) serve as illustrative examples of polyols used as starting reagents along with diisocyanates for PIL synthesis [26,27,29]. In the case of polyurethane (PU)-based cationic PILs, the respective ILs in the form of diols are employed, thus incorporating the IL cation into the polymer chain as documented in the literature [26,29,30]. This study endeavors to synthesize and evaluate the CO_2/CH_4 separation potential of PU-based cationic PIL membranes. The IL GLYMIM[Cl] was synthesized, followed by ion exchange processes to obtain GLYMIM with different counter anions (NTf_2^-, PF_6^- and BF_4^-). These ILs were used as diols in the synthesis of PILs, aiming to tailor polymeric chains with high affinity for CO_2, thereby producing membranes with improved selectivity.

2. Materials and Methods

2.1. Materials

For the synthesis of hydroxyl-functionalized ionic liquids (ILs), N-methylimidazole (Sigma-Aldrich, Burlington, MA, USA), 3-chloro-1,2-propanediol (Sigma-Aldrich), ethyl acetate (Neon Química, São Paulo, Brazil), lithium bis(trifluoromethanesulfonyl)imide ($LiNT_2F$, Sigma-Aldrich, USA), lithium tetrafluoroborate ($LiBF_4$, Sigma-Aldrich, USA), and sodium hexafluorophosphate ($NaPF_6$, Sigma-Aldrich, USA) were used. To obtain the PILs, polycarbonate diol (PCD, Mn = 2000 g/mol, Bayer, Berlin, Germany), hexamethylene diisocyanate (HDI, 99%, Merck, Darmstadt, Germany), dibutyltin dilaurate (DBTDL, Miracema Nuodex, Campinas, Brazil), methyl ethylketone (MEK, 99%, Mallinckrodt, Hazelwood, MO, USA) and the obtained ILs glyceryl-N-methylimidazolium chloride [GLYMIM][Cl], and derivatives ([GLYMIM][Cl], [GLYMIM][NT_2F], ([GLYMIM][BF_4] and ([GLYMIM][PF_6]) were used.

2.2. Synthesis of Hydroxyl-Functionalized Ionic Liquids

The synthesis of glyceryl-N-methylimidazolium chloride was conducted as described in the literature [25,31,32]. The reaction was carried out continuously in a glycerin bath with constant magnetic stirring at a temperature of 70 °C. During the first hour of the

reaction, 10 mL (0.11 mol) of 3-chloro-1,2-propanediol was slowly added dropwise to a solution containing 12 mL (0.15 mol) of N-methylimidazole. The reaction conditions were maintained for 72 h.

Subsequently, the reaction mixture was removed from the heat and washed six times with ethyl acetate. The resulting material was then placed in a glycerin bath to maintain a constant temperature of 70 °C and dried under vacuum for 24 h.

The product was stored under a nitrogen atmosphere, resulting in a yellow oil [25,31,32]. Ion exchanges were performed in acetonitrile by reacting [GLYMIM]Cl with the respective salts: $LiNT_2F$ to obtain [GLYMIM]NT_2F, $LiBF_4$ to form [GLYMIM]BF_4, and $NaPF_6$ to form [GLYMIM]PF_6. It should be noted that the reagents used in the ion exchange process ([GLYMIM]Cl, $LiBF_4$, $LiNT_2F$, and $NaPF_6$) are soluble in acetonitrile, while the by-products, LiCl and NaCl, are not soluble. This allowed for easy separation of the by-products through simple filtration [25,32–34]. The obtained structures can be observed in Figure 1.

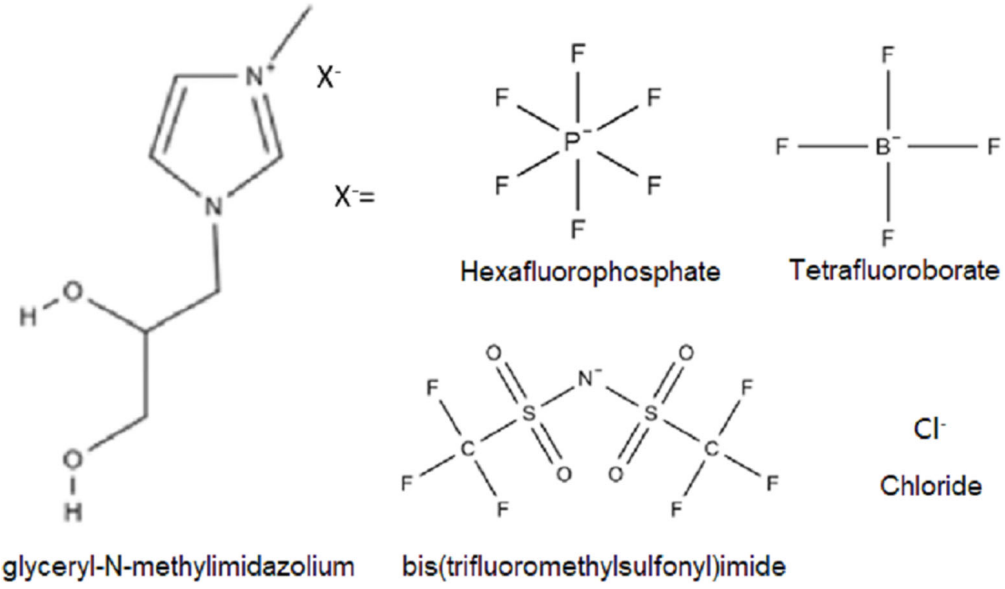

Figure 1. ILs structure.

$AgNO_3$ tests were carried out until no significant amount of white precipitate was observed, confirming satisfactory removal of the by-product. Vacuum drying was then performed to remove any excess solvent and moisture.

2.3. Cationic Poly(Ionic Liquids)

Initially, under constant stirring, the polyol PCD (0.04 mol) was melted in a five-neck reactor, the DBTDL catalyst (0.1% by weight) was added, and 50 mL of methyl ethyl ketone was added. After reaching the reaction temperature (70 °C), the diisocyanate (0.047 mol) was added to form the prepolymer. Then, dialcohol ([GLYMIM]Cl) (0.11 mol) and diisocyanate (0.11 mol) were added to form the PIL. The completion of the reaction is indicated by the disappearance of the free NCO band (around 2270 cm^{-1}) in the infrared spectrum. The synthesized PILs were labeled as PLIX, where X represents the counteranion (Cl, NT_2F, PF_6, or BF_4). Figure 2 shows the structural formula of a cationic PIL.

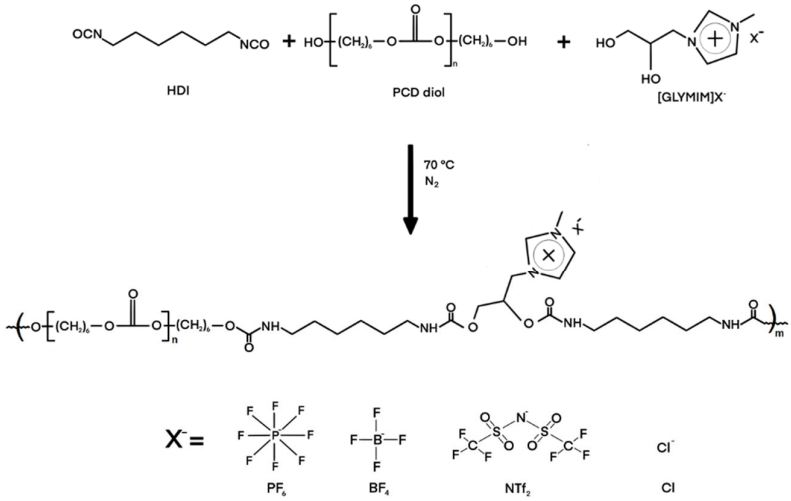

Figure 2. Structures of the cationic PILs.

2.4. Syntheses of PU

The PU preparation process was the same as the method used for the synthesis of cationic poly(ionic liquid); however, [GLYMIM]X, was not added, using an NCO/OH molar ratio of 1.1.

2.5. Preparation of Dense Membranes

Membranes were prepared using the casting or solvent evaporation method with thickness between 150 and 250 μm. Initially, a 20% *w*/*w* solution of PU or PIL was prepared by dissolving 2 g of PIL in 10 mL of methyl ethylketone by magnetic stirring and heating (50 °C) until the PIL was completely dissolved. The solution was then applied to a flat surface, such as a glass plate or a Petri dish, followed by solvent evaporation at room temperature for five days.

2.6. Characterization

Hydroxyl-functionalized ILs and synthesized PILs were characterized by Fourier transform infrared spectroscopy (FTIR, PerkinElmer Spectrum 100 spectrometer, PerkinElmer, Waltham, MA, USA) in transmission mode in the range of 4000–650 cm^{-1} to verify their structures. The synthesized ILs were also characterized by nuclear magnetic resonance (NMR) using a Bruker Ascend 400 model NMR spectrometer, Bruker, Billerica, MA, USA.

The molar masses of the PIL membranes and their distribution were determined by gel permeation chromatography (GPC), with chromatograms obtained using the isocratic HPLC pump-1515 chromatograph (LabMakelaar Benelux, Zevenhuizen, The Netherlands) coupled with a Waters Instruments 2412 (Waters Corp, Milford, CT, USA) refractive index detector and THF as eluent.

Scanning electron microscopy with field emission (FEI Inspect F50, FEI Company, Hillsboro, OR, USA) analyses were performed in secondary electrons (SE) mode to evaluate the surface of the composite membranes.

Differential scanning calorimetry (DSC, TA Instruments Q20, TA Instruments, New Castle, DE, USA) was used to determine the glass transition temperature (Tg), melting temperature (Tm), and crystallization temperature (Tc) of the PILs. Tests were performed with two heating ramps and one cooling ramp in the range of −90 to 200 °C at 10 °C/min under an inert nitrogen atmosphere.

The thermal stability of the PILs was assessed through thermogravimetric analysis (TGA) using a TA Instruments Q600 model instrument, ranging from room temperature to 600 °C with a heating rate of 10 °C/min under a nitrogen atmosphere.

Mechanical analyses were performed in triplicate according to ASTM D822 standard [35] on a TA Instruments Q800 (TA Instruments, New Castle, DE, USA) apparatus to determine Young's moduli and obtain stress–strain curves.

2.7. CO_2 Sorption Capacity

The pressure decay technique was used to determine the CO_2 sorption capacity. A detailed description of the sorption apparatus and measurement procedure can be found in our previous works [26,27]. Samples (1.0 g) were placed in the sorption chamber and degassed under vacuum (10^{-3} mbar) for 1 h at room temperature before the test began. CO_2 sorption experiments were carried out at 30 °C at different equilibrium pressures (1 bar and 10 bar).

2.8. CO_2 Permeability and Ideal CO_2/CH_4 Selectivity

The permeation and selectivity for CO_2 and CH_4 of the PLI membranes were evaluated in a system consisting of two plates joined in a 4 cm diameter hole (Figure S1), where the membrane is inserted. Vacuum was applied to the membrane and the system before gas feed. CO_2 or CH_4 was fed at a pressure of 4 bar. At the bottom, a pressure transducer computed the amount of gas passing through the membrane over time (dp/dt). The permeate gas was assumed to exhibit ideal behavior; therefore, normal temperature and pressure conditions were used. Permeability was determined from the slope (dp/dt) of the linear portion of pressure versus time using Equation (1):

$$\frac{P}{l} = \frac{dp}{dt}\left(\frac{V_{System}}{A\ \Delta p}\right)\left(\frac{T_{CNTP}}{T\ P_{CNTP}}\right) \quad (1)$$

where l is the membrane thickness, P is permeability, Δp is the pressure difference across the membrane, A corresponds to the membrane area, V_{System} is the volume of the permeation cell, T is the ambient temperature, and T_{CNTP} and P_{CNTP} are, respectively, the temperature and pressure at normal conditions [36]. The ideal selectivity was calculated from Equation (2) by dividing the CO_2 permeability by the CH_4 permeability.

$$\propto_{CO_2/CH_4} = \frac{P_{CO_2}}{P_{CH_4}} \quad (2)$$

The solution-diffusion mechanism is widely accepted as the primary transport mechanism for gas permeation through a dense membrane [37,38]. In this mechanism, the gas solubility coefficient (cm^3(STP)/(cm^3 cmHg)) is calculated using Equation (3):

$$S = \frac{P}{D} \quad (3)$$

where P represents permeability and D represents the gas diffusion coefficient (cm^2/s). The gas diffusion coefficient was determined using the time-lag method described by Equation (4) [37,39]:

$$D = \frac{l^2}{6\theta} \quad (4)$$

where D is the diffusion coefficient (cm^2/s), l is the membrane thickness (cm), and θ is the diffusion time lag (s) determined by the linear portion of the curve intercepting the time axis.

3. Results

3.1. Characterization of the ILs

Figure S2 shows the FTIR spectra of the ILs. The IL [GLYMIM]Cl exhibited the expected bands confirming the desired product formation. The OH band between 3281 and 3239 cm^{-1} was visible, as well as bands related to the imidazolium ring near 1670 cm^{-1}

(C=C), 1604 cm^{-1} (N-H), and 1371 cm^{-1} (aromatic C-N) [25,40]. The substitution of the Cl anion by NT_2F resulted in the appearance of bands between 1200 cm^{-1} and 1400 cm^{-1}, characteristic for this ion, as well as others near 1060 cm^{-1} corresponding to S=O bonds, 846 cm^{-1} corresponding to N-S bonds, 789 cm^{-1} corresponding to C-S bonds, and 751 cm^{-1} corresponding to C-F bonds. Substitution of Cl by BF_4 and PF_6 anions also caused changes in the spectra, resulting in the appearance of bands at 815 cm^{-1} for PF_6 P-F bonds and at 1050 cm^{-1} for BF_4 B-F bonds [41–43].

For illustrative purposes, the NMR spectra of the chloride-functionalized N-glyceryl-N-methylimidazole [GLYMIM]Cl (Figure S3) and [GLYMIM]NT_2F (Figure S4) ILs, obtained after the exchange of the chloride anion (Cl^-) for NT_2F, are shown. The 1H NMR spectrum (DMSO-d6) of [GLYMIM]Cl (Figure S2) exhibited characteristic peaks: 3.4 ppm (2H, CH2), 3.7 ppm (1H, CH), 3.9 ppm (3H, CH3), 4.4 ppm (2H, CH2), 5.3 ppm (1H, OH), 5.6 ppm (1H, OH), 7.7 ppm (1H, CH), 7.8 ppm (1H, CH), and 9.2 ppm (1H, CH) [25,32,44]. The 13C spectrum (DMSO-d6) of [GLYMIM]NT_2F (Figure S3) showed characteristic peaks: δ 36.1 (CH_3); 52.5 (-N+CH_2); 63.1 (CH_2OH); 70.07 (CHOH); 123.5 (CH); 123.6 (CH); 137.5 (CH); and 117.4 (2C, NT_2F) [25,32,44].

3.2. Characterization of Cationic Poly(Ionic Liquids)

The molecular weight distributions (PD, polydispersity) and the weighted molecular weights (Mw) of the PILs are presented in Table S1. The Mw values ranged from 43,264 $gmol^{-1}$ to 70,655 $gmol^{-1}$, while the polydispersity (PD) ranged from 1.2 to 1.4. In Figure 3, spectra obtained for the PILs are shown, and Figure 4 shows the enlargements of the spectra in the regions of 3000–3700 cm^{-1}; 1600–1800 cm^{-1}; and 650–1350 cm^{-1}. FTIR spectra (Figure 3) showed characteristic bands found for polyurethanes: 2936–2871 cm^{-1} (CH_2 and CH_3 stretching), 1536 cm^{-1} (N–H bending groups), 1246 cm^{-1} (vibration of C-N and C-O groups of urethane), 1041 cm^{-1} (stretching of C–O–C groups of urethane), and 955 cm^{-1} (stretching of C–O–C groups of polycarbonate diol) [45]. The bands characteristic of H bonds present in polyurethanes were also evaluated: the region between 3200 and 3500 cm^{-1} corresponding to the stretching vibration of the N-H group of urethane (Figure 4A) and the region between 1700 and 1730 cm^{-1} characteristic of bonded and non-bonded carbonyl groups, respectively (Figure 4B). Shifts in characteristic bands (N-H and C=O) evidence possible H bonds. Figure 4A shows the characteristic bands of the stretching vibration of urethane N-H groups, where the region around 3400 cm^{-1} corresponds to non-bonded N-H groups and the band in the region of 3300 cm^{-1} characterizes the vibration of bonded N-H groups. All PILs showed an increase in intensity in the regions of bonded and non-bonded N-H groups with the insertion of IL into the polymeric chain. Also, concerning the structure of polyurethane, Figure 4B contains an enlargement of this area between 1600 and 1800 cm^{-1}. In this range, it is possible to observe bands related to non-bonded carbonyl groups near 1730 cm^{-1} and bonded carbonyl groups near 1700 cm^{-1} [27]. In Figure 4B, changes in the spectrum were also noticed only when IL insertion is performed, such as the displacement of the band ~1730 cm^{-1} to values close to ~1710 cm^{-1}. The appearance of characteristic bands of bonded carbonyl groups in the regions of 1700 cm^{-1} for samples with Cl, PF_6 and BF_4, and 1650 cm^{-1} for samples with NTf_2, PF_6, and BF_4 counterions was observed, indicating the formation of H bonds [26,27]. The absence of the characteristic band for the stretching vibration of the N=C=O group in the region of 2270 cm^{-1} confirms the absence of free NCO groups in the polymeric material, indicating the formation of PU [27,29,46]. Bands related to the counter anions present in the samples can also be visualized (Figure 3). The PIL-BF4 sample presents a broad band near 1060 cm^{-1}, indicating the presence of the B-F bond [41–43]. The PIL-PF_6 presents a band near 835 cm^{-1} related to P-F bonds. For PIL-NTf_2, a band near 1346 cm^{-1} related to SO_2 bond vibrations was observed, as well as bands near 1136 cm^{-1} and 1189 cm^{-1} related to C-F bond vibrations [41–43].

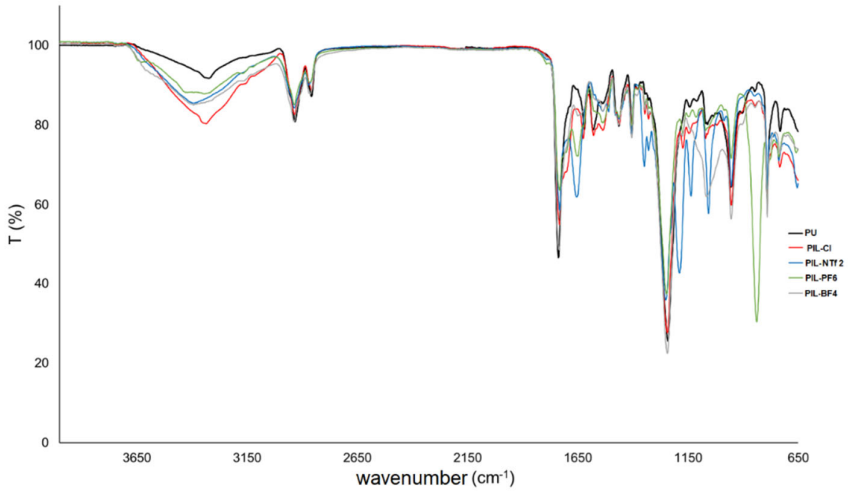

Figure 3. Infrared spectra of PU and cationic PILs.

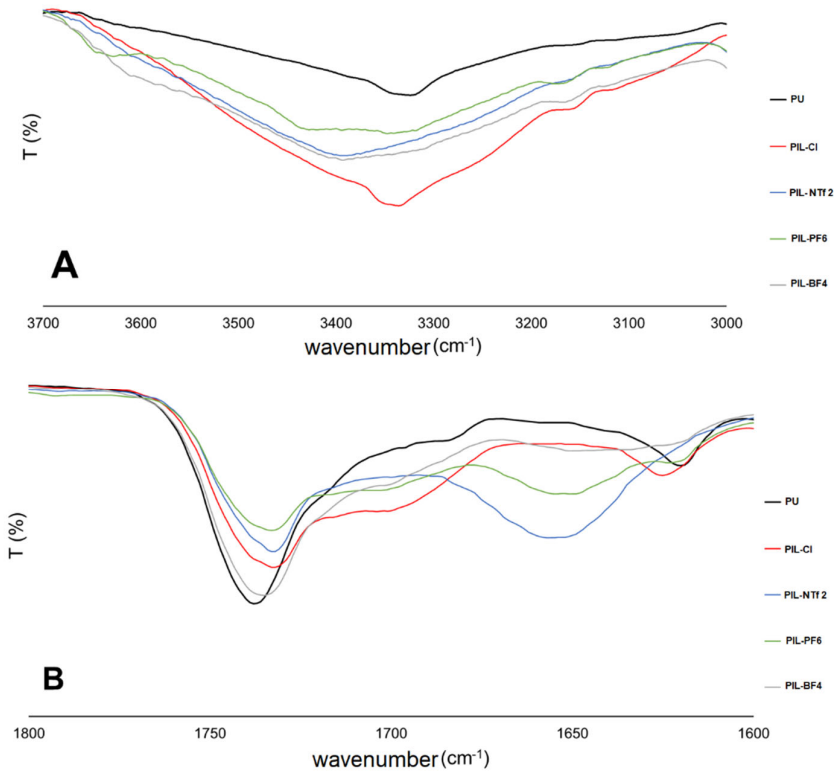

Figure 4. Infrared spectra of PU and cationic PILs. (**A**) 3000–3700 cm^{-1}; (**B**) 1600–1800 cm^{-1}.

3.2.1. DSC

The DSC curves obtained for the polymeric samples are presented in Figure 5. The glass transition temperatures (Tg) values of −44.7, −47.9, −43.2, and −42.7 °C were found for the samples PIL-Cl, PIL-NTf_2, PIL-PF_6, and PIL-BF_4, respectively. By comparing the values obtained for the PILs with the result obtained for pure PU (−42 °C), it is possible to perceive a decreased tendency in the Tg values for all PILs in relation to the non-ionic PU, which could mean that the addition of ILs in the polymeric chain increases the separation of the polymer microphases. This separation of microphases facilitates the mobility of the chains [26,27]. From the analysis of the thermograms, it is possible to identify the existence of an endothermic peak which can be attributed to the melting of a crystalline microphase (Tmf). This endothermic peak is characteristic for PU-based polymers that use polyol PCD with a molecular weight of 2000 g/mol in the polymer chain [26,27]. The results found for

the PU, PIL-Cl, PIL-NTf_2, PIL-PF_6, and PIL-BF_4 samples were, respectively, 40.1 °C, 42.2 °C, 46.4 °C, 42.8 °C, and 43.5 °C. Finally, the crystallization temperature (Tc) was obtained for the PIL-Cl sample (−12.7 °C).

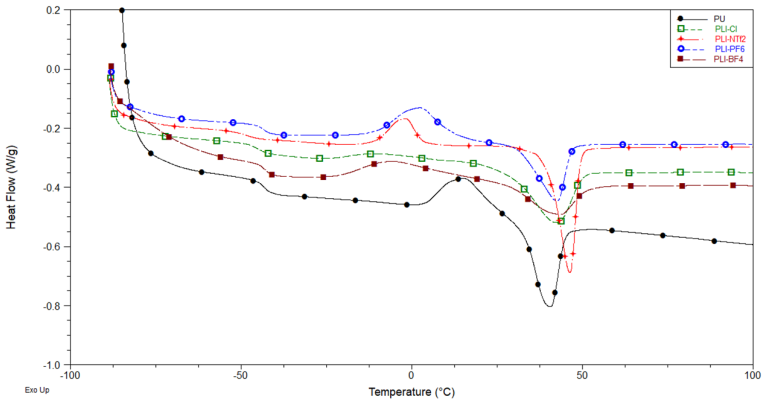

Figure 5. DSC curves of the PILs.

3.2.2. TGA

Table 1 and Figure S5 present the results of the degradation temperature obtained by TGA. PIL samples showed their first degradation temperature between 279 °C and 325 °C. This initial decomposition temperature corresponds to the rigid segments, where the degradation of the polyurethane bonds occurs. The second stage occurs around 440–469 °C, which refers to the breakdown of the flexible segments, leading to the degradation of the polyol along with the imidazole molecules. The incorporation of ILs led to an increase in the decomposition temperature, which may be related to the hydrogen bonds that may occur between PU and IL. Thermal decomposition of ILs typically occurs between 200 and 350 °C, suggesting that the decomposition of ILs may be occurring in the first stage of PILs degradation [47–49].

Table 1. Results of degradation temperatures obtained by TGA.

Sample	T_{onset1} (°C)	T_{onset2} (°C)
PU	276	428
PIL-Cl	279	469
PIL-NTf_2	318	462
PIL-PF_6	300	440
PIL-BF_4	325	445

3.2.3. DMA

Figure 6 shows the stress–strain curves referring to the PILs samples. In terms of Young's modulus, the increasing order is PIL-NTf_2 < PIL-Cl < PIL-PF_6 < PIL-BF_4 < PU. The Young's modulus values obtained for the PILs samples were 7 MPa (PIL-NTf_2), 16.4 MPa (PIL-Cl), 29 MPa (PIL-PF_6), 47 MPa (PIL-BF_4), and 53 MPa (PU). The insertion of an IL into the polymeric chain can act as a plasticizer, interfering with the flexibility and mobility of the chains, affecting the Young's modulus and resulting in its decrease [27,47]. Another possibility for this material behavior is the increased separation of the polymer microphases, which can also lead to a decrease in the Young's modulus and elongation of the curve [50,51]. Except for PIL-NTf_2, it can be observed that, besides the decrease in Young's modulus, which indicates greater elasticity of the material, the curve becomes more elongated when comparing the PIL samples with the non-ionic PU sample.

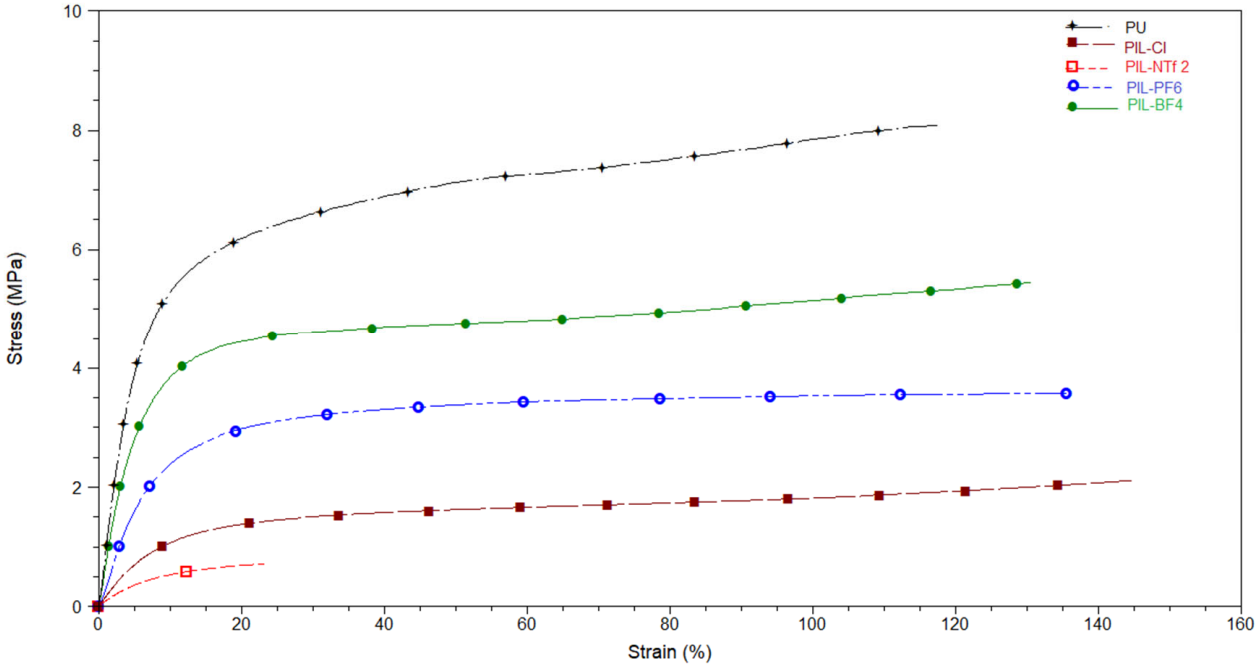

Figure 6. Stress–strain curves of PU and cationic PILs.

3.3. CO_2 Sorption Capacity

The CO_2 capture results can be observed in Figure 7. From the values found, it can be noticed that increasing pressure also increases the amount of captured CO_2. This behavior is typical of samples that undergo CO_2 sorption through physical interaction, as is the case with the PILs obtained in this work. The results obtained for the non-ionic PU sample were 24.7 mg CO_2/g (1 bar) and 83.1 mg CO_2/g (10 bar). These CO_2 capture results before the addition of the ionic liquid can be attributed to the interactions between CO_2 and the polar groups composed of nitrogen and oxygen present in the structure of the PU polymer chain. Additionally, Figure 7 shows that the insertion of the IL leads to a slight increase in CO_2 capture values for all PIL samples. The results obtained for 1 bar were 27.5 mg CO_2/g for PIL-PF_6, 26.3 mg CO_2/g for PIL-Cl, 27.6 mg CO_2/g for PIL-NTf_2, and 33.5 mg CO_2/g for PIL-BF_4. For the same samples at 10 bar, the results were 93.7 mg CO_2/g for PLI-PC-Cl, 95.4 mg CO_2/g for PLI-PC-PF6, 98.1 mg CO_2/g for PIL-NTf_2, and 104.8 mg CO_2/g for PIL-BF_4. The sorption capacity increases in the following order: $[Cl]^-$ < $[PF_6]^-$ < $[NTf_2]^-$ < $[BF_4]^-$ for 1 and 10 bar. As expected, fluorinated anions showed a higher affinity for CO_2. However, in this case, the size of the anion also appears to influence the CO_2 sorption capacity. The structures of the NTF_2^- and PF_6^- anions are larger when compared to the BF_4^- [41,52]. This may block some important CO_2 interaction sites in the PIL cation, reducing the sorption capacity [53]. In the tests conducted, the CO_2 sorption capacity of PIL-BF_4 was superior compared to PU-based PILs reported in the literature using the BF_4 anion. For example, Morozova 2017 [29] and Morozova 2020 [28] obtained 24.7 mgCO_2/g for the PIL-8.1.BF_4 and 24.8 mgCO_2/g for PUR2.BF_4 at 1 bar and 273 K.

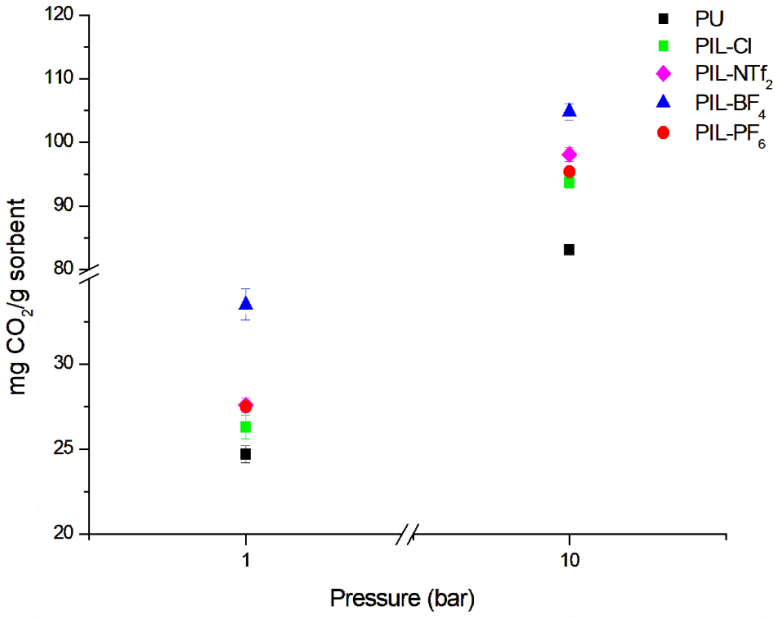

Figure 7. Sorption results for PU and cationic PILs at 1 and 10 bar with a temperature of 303.15 K.

3.4. Permeability and CO_2 Selectivity

Table 2 presents the results of the CO_2 permeability and ideal (CO_2/CH_4) selectivity obtained for dense membranes of cationic PILs and pristine PU, compared to the results of cellulose acetate and some PILs found in the literature. The incorporation of ILs into the polymer chains produced membranes with superior performance when compared to neat PU, as seen in Table 2. It is observed that PIL-CL and PIL-BF_4 samples tested exhibited higher CO_2/CH_4 selectivity than cellulose acetate [54,55]. Furthermore, it can be highlighted that the PIL-BF_4 sample showed the best permeability and selectivity results among all samples presented in Table 2. The PIL-NTf_2 sample presents poor mechanical properties, breaking during the test. Better CO_2 permeability is expected for PILs, as the diffusion and solubility of CO_2 molecules are generally high in ionic liquids [56]. The influence of PIL anions on CO_2 affinity is well documented in the literature [53] and corroborated in our experiments. Permeability and selectivity increased when the Cl^- anion was replaced by BF_4^-, indicating that the presence of fluorine in PILs can enhance CO_2 affinity. However, interestingly, the PF_6^- anion showed lower permeability and selectivity compared to the other anions. This behavior may be related to the size of the anion. The sizes of the anions used in this work follow the general trend $Cl^- < BF_4^- < PF_6^- < NTF_2^-$ [41,52]. Therefore, although BF_4^- and PF_6^- have similar structures, PF_6 has a larger size. Bulky anion structures can reduce the free volume of the PIL, hindering CO_2 penetration towards the cation, which is primarily responsible for sorption [53]. According to Vollas et al. [41], the presence of smaller anions such as $BF4^-$ facilitates polymer packing through chain interactions, leading to denser structures and consequently lower methane permeabilities. Therefore, there appears to be an optimal size for fluorinated anions (BF_4^-) to achieve high permeability and selectivity.

Table 2. Permeability and ideal selectivity results for cationic PILs (25 °C and 4 bar), compared with results for cellulose acetate and PILs from the literature.

Membrane	Perm. CO_2 (Barrer)	Perm. CH_4 (Barrer)	Sel. Ideal CO_2/CH_4
PU	2.0 ± 0.1	0.78 ± 0.02	2.5
PIL-Cl	17 ± 2.2	0.6 ± 0.1	30
PIL-NTf_2	-	-	-
PIL-PF_6	9 ± 1.7	0.6 ± 0.2	14
PIL-BF_4	41 ± 3.2	0.9 ± 0.3	44
1—CTA (25 °C, 5 bar)	18	1.98	9
2—CA (25 °C, 3 bar)	15	1.45	10
3—CA (25 °C, 1 bar)	4	0.2	17
4—CA (35° C, 3 bar)	4.3	0.21	21
5—Styrene-Based Poly(RTILS) (2 atm; RT)	9.2 ± 0.5	0.24 ± 0.01	39
5—Acrylate-Based Poly(RTILS) (2 atm; RT)	7.0 ± 0.4	0.19 ± 0.02	37
6—PIL-TFSI (1 atm; RT)	4.1 ± 0.1	-	41
7—OEG_1 (2 atm; 295 K)	16 ± 1	0.48 ± 0.01	33
7—OEG_2 (2 atm; 295 K)	22 ± 1	0.74 ± 0.02	29
8—PIL-i-propyl (3 atm; 20 °C)	10.4 ± 0.2	0.35 ± 0.01	30
9—Poly[DPyDBzPBI-BuI][Tf2N] (20 atm; 35 °C)	36.2	1.25	29

1—Raza, A. et al., 2021 [54]; 2—Mubashir, M. et al., 2018 [55]; 3—Saijan, P. et al., 2020 [57]; 4—Akbarzadeh, E. et al., 2021 [58]; 5—Bara, J. et al., 2007 [59]; 6—Vollas, A. et al., 2018 [41]; 7—Bara, J. et al., 2008 [60]; 8—Horne, W. et al., 2015 [61]; 9—Shaligram, S. et al., 2016 [62].

To obtain more information about the gas transport mechanism through the membranes, the diffusion and solubility coefficients for CO_2 were determined. These coefficients can provide a better understanding of the variations in permeability obtained for the different PILs, as presented in Table 2. Furthermore, these coefficients can offer a better understanding of the permeability variations of PIL membranes with different counter anions, as presented in Table 3. The values of the diffusion and solubility coefficients showed that the obtained PIL membranes exhibited higher diffusivity and solubility to CO_2 than to CH_4, which contributed to the achieved CO_2 permeabilities. Additionally, this behavior may be related to the high affinity of ILs with the polar groups of CO_2. It can be highlighted that the PIL-BF_4 sample showed higher diffusion and solubility coefficients, corroborating with the sorption capacity results. It is known that CO_2 solubility is influenced by various factors, such as the size of the anions, which can lead to an increase in the free volume of PIL, thus enhancing gas solubility since there is more space available for sorption [63].

Table 3. Diffusion and solubility coefficients for PIL membranes at 4 bar and 25 °C.

Membrane	D (10^{-8} cm²/s)		S (10^{-2} cm³(STP)/(cm³ cmHg))		$D_{CO2/CH4}$	$S_{CO2/CH4}$
	CO_2	CH_4	CO_2	CH_4		
PIL-Cl	21.60	2.32	0.78	0.26	9.32	3.04
PIL-NTf_2	-	-	-	-	-	-
PIL-PF_6	22.04	1.61	0.41	0.37	13.68	1.10
PIL-BF_4	32.67	1.79	1.26	0.50	18.22	2.52
CA (35 °C, 3 bar) [57]	2.05	0.55	2.11	0.38	3.72	5.55

3.5. Comparison with Robeson Upper Bound

The separation performance of dense cationic PIL membranes in this study was compared with Robeson's curves for CO_2/CH_4 [64,65], as shown in Figure 8. It can be observed that the membranes achieved performance below the Robeson limit; however, the PIL-BF_4 sample is better positioned when compared to samples with Cl^- and PF_6^- anions, being very close to the upper limit of 1991. A likely explanation lies in the relatively low CO_2 permeability of the PILs with Cl^- and PF_6^- anions, although they show superior results compared to commercial polymer cellulose acetate. The highlight of the PIL-BF_4

sample is the ideal selectivity for CO_2/CH_4, which is higher than in other studies reported in the literature [66].

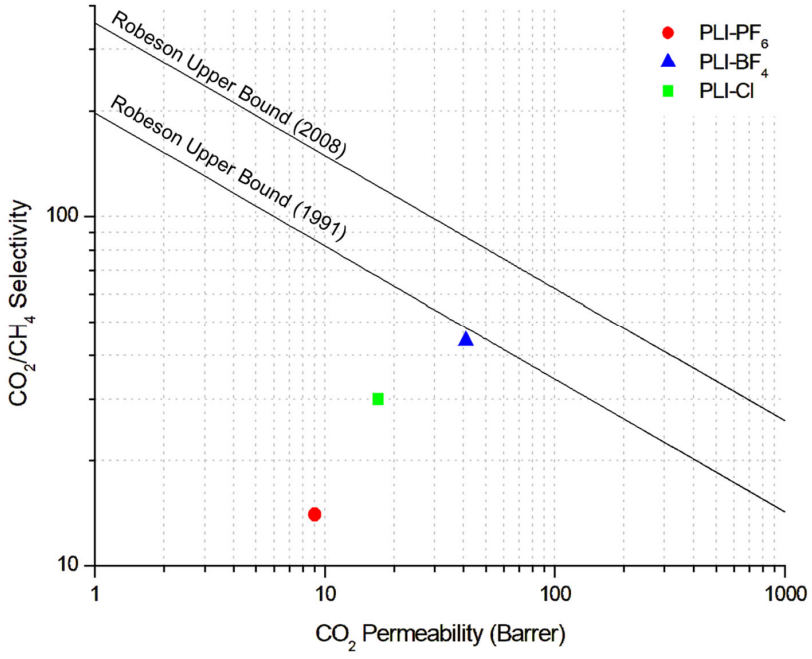

Figure 8. Performance of cationic PIL membranes at the Robeson upper bound for CO_2/CH_4 separation.

In this context, the obtained permeability and ideal selectivity results demonstrate that the synthesized PIL membranes are extremely promising for CO_2/CH_4 separation, especially because there is an intention to explore structural modification of the polymer chain to enhance the permeability and selectivity of these membranes [41]. It can be observed that the samples of cationic PILs prepared with different counter anions exhibited good permeability and high selectivity for CO_2. From the SEM images shown in Figure 9, it can be seen that the PIL membranes produced for the permeability tests exhibited a surface without pores and defects.

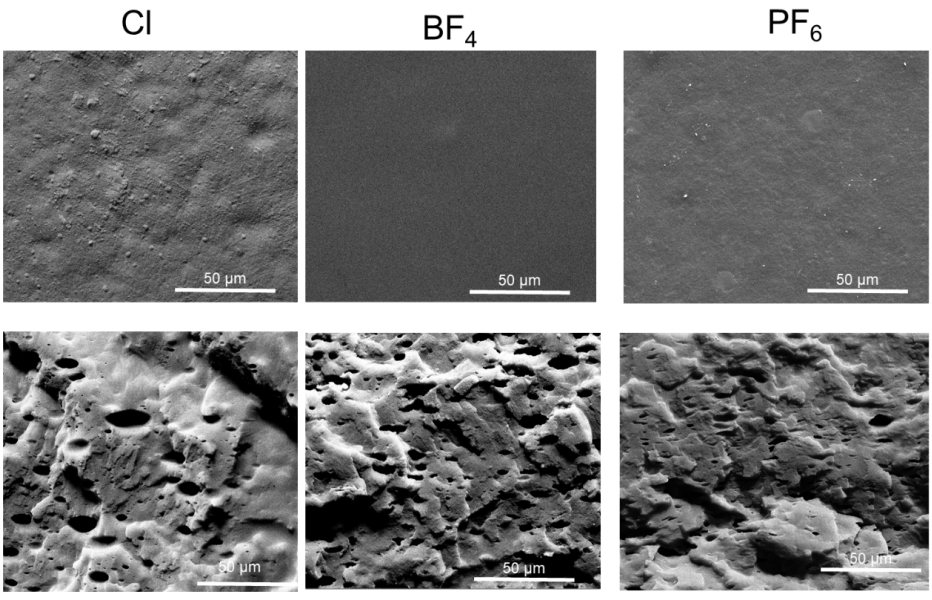

Figure 9. Surface and cross-sectional micrographs (cryogenic fracture) of PIL membranes, magnification, 3000×.

4. Conclusions

In this study, we successfully developed PIL membranes that exhibited adequate thermal and mechanical properties, high CO_2 permeability, and ideal CO_2/CH_4 selectivity. The IL GLYMIM [Cl] was synthesized and thoroughly characterized, and different counter anions' chemical structures (NTf_2, PF_6, and BF_4) were evaluated to identify the optimal combination for physicochemical properties, sorption, and permeability. FTIR analysis confirmed the presence of the characteristic bands for both ILs and PILs. The incorporation of IL into the polymer chain resulted in a decrease in the Tg values, indicating improved membrane flexibility. Among the samples tested, PIL-BF_4 demonstrated the best performance in terms of sorption, permeability, and ideal CO_2/CH_4 selectivity. This suggests that appropriately sized fluorinated anions significantly enhance CO_2 permeability and ideal CO_2/CH_4 selectivity, outperforming the commercial cellulose acetate membrane.

Supplementary Materials: The following supporting information can be downloaded at: https://www.mdpi.com/article/10.3390/membranes14070151/s1, Figure S1: Illustration of permeability system set up; Figure S2: Synthesized ionic liquids spectra; Figure S3: IL ([GLYMIM]) Cl RMN spectra, 1H (DMSO-d6); Figure S4: IL [GLYMIM]NT2F 13C RMN spectra; Figure S5: PILs TGA curves; Table S1: PILs GPC results.

Author Contributions: Conceptualization, S.E., G.D. and F.L.B.; methodology, G.D., L.R., H.Z.F. and F.L.B.; validation, G.D., L.R., H.Z.F. and F.L.B.; formal analysis, S.E., F.L.B., L.P., G.D, L.R., H.Z.F. and F.G.B.; investigation, S.E., F.L.B., L.P., G.D., L.R., H.Z.F. and F.B; resources, S.E., F.L.B., F.G.B. and L.P.; data curation, S.E., F.L.B., L.P., G.D., L.R., H.Z.F. and F.G.B.; writing—original draft preparation, G.D., F.L.B., H.Z.F. and S.E. writing—review and editing, G.D., F.L.B., H.Z.F. and S.E.; supervision, S.E.; project administration, S.E. and F.G.B.; funding acquisition, S.E., F.L.B. and F.G.B. All authors have read and agreed to the published version of the manuscript.

Funding: This research was founded by Petrobras Project Number 4600677123 and CNPq Project Number 316580/2021-0.

Institutional Review Board Statement: Not applicable.

Data Availability Statement: The original contributions presented in the study are included in the article, further inquiries can be directed to the corresponding author.

Acknowledgments: The authors would like to thank PETROBRAS for financial support; Sandra Einloft thanks CNPq for research scholarship.

Conflicts of Interest: Author Fernando Brandão and Leonardo Pereira were employed by the company Petrobras. The remaining authors declare that the research was conducted in the absence of any commercial or financial relationships that could be construed as a potential conflict of interest.

Nomenclature

PILs	poly(ionic liquids) or polymerized ionic liquids
ILs	ionic liquids
GLYMIM	glyceryl-N-methylimidazolium
Cl^-	chloride anion
NTf_2^-	bis(trifluoromethanesulfonyl)imide anion
PF_6^-	hexafluorophosphate
BF_4^-	tetrafluoroborate
PU	polyurethane
PTMG	polytetramethylene glycol
PCD	polycarbonate diol
PCL	polycaprolactone
HDI	hexamethylene diisocyanate
DBTDL	dibutyltin dilaurate
MEK	methyl ethylketone
PD	polydispersity

Mw	molecular weights
Tg	glass transition temperatures

References

1. Supasitmongkol, S.; Styring, P. High CO_2 Solubility in Ionic Liquids and a Tetraalkylammonium-Based Poly(Ionic Liquid). *Energy Environ. Sci.* **2010**, *3*, 1961–1972. [CrossRef]
2. Privalova, E.I.; Mäki-Arvela, P.; Murzin, D.Y.; Mikkhola, J.P. Capturing CO_2: Conventional versus Ionic-Liquid Based Technologies. *Russ. Chem. Rev.* **2012**, *81*, 435–457. [CrossRef]
3. Rockett, G.C. Associação de Fontes Emissoras e Reservatórios Potenciais para Armazenamento Geológico de CO_2 na Bacia de Campos, Brasil. Bachelor's Thesis, Pontifical Catholic University of Rio Grande do Sul, Porto Alegre, Brazil, 2010.
4. Dunn, C.A.; Denning, S.; Crawford, J.M.; Zhou, R.; Dwulet, G.E.; Carreon, M.A.; Gin, D.L.; Noble, R.D. CO_2/CH_4 Separation Characteristics of Poly(RTIL)-RTIL-Zeolite Mixed-Matrix Membranes Evaluated under Binary Feeds up to 40 Bar and 50 °C. *J. Memb. Sci.* **2021**, *621*, 118979. [CrossRef]
5. Aghaie, M.; Rezaei, N.; Zendehboudi, S. A Systematic Review on CO_2 Capture with Ionic Liquids: Current Status and Future Prospects. *Renew. Sustain. Energy Rev.* **2018**, *96*, 502–525. [CrossRef]
6. Privalova, E.I.; Karjalainen, E.; Nurmi, M.; Mäki-Arvela, P.; Eränen, K.; Tenhu, H.; Murzin, D.Y.; Mikkola, J.P. Imidazolium-Based Poly(Ionic Liquid)s as New Alternatives for CO_2 Capture. *ChemSusChem* **2013**, *6*, 1500–1509. [CrossRef] [PubMed]
7. Luis, P. Use of Monoethanolamine (MEA) for CO_2 Capture in a Global Scenario: Consequences and Alternatives. *Desalination* **2016**, *380*, 93–99. [CrossRef]
8. Kwak, N.S.; Lee, J.H.; Lee, I.Y.; Jang, K.R.; Shim, J.G. A Study of the CO_2 Capture Pilot Plant by Amine Absorption. *Energy* **2012**, *47*, 41–46. [CrossRef]
9. Panahi, M.; Skogestad, S. Economically Efficient Operation of CO_2 Capturing Process Part I: Self-Optimizing Procedure for Selecting the Best Controlled Variables. *Chem. Eng. Process. Process Intensif.* **2011**, *50*, 247–253. [CrossRef]
10. Kausar, A.; Nulwala, H.; Mirjafari, A.; Zhou, X.; Duan, N.; Sun, Z.; Ren, Y.; Liu, Z.; Liu, L.; Yan, F.; et al. Enhanced CO_2 Absorption of Poly(Ionic Liquid)s. *Macromolecules* **2021**, *38*, 5477–5489. [CrossRef]
11. Idem, R.; Wilson, M.; Tontiwachwuthikul, P.; Chakma, A.; Veawab, A.; Aroonwilas, A.; Gelowitz, D. Pilot Plant Studies of the CO_2 Capture Performance of Aqueous MEA and Mixed MEA/MDEA Solvents at the University of Regina CO_2 Capture Technology Development Plant and the Boundary Dam CO_2 Capture Demonstration Plant. *Ind. Eng. Chem. Res.* **2006**, *45*, 2414–2420. [CrossRef]
12. Liang, Z.; Rongwong, W.; Liu, H.; Fu, K.; Gao, H.; Cao, F.; Zhang, R.; Sema, T.; Henni, A.; Sumon, K.; et al. Recent Progress and New Developments in Post-Combustion Carbon-Capture Technology with Amine Based Solvents. *Int. J. Greenh. Gas Control.* **2015**, *40*, 26–54. [CrossRef]
13. Lei, Z.; Dai, C.; Chen, B. Gas Solubility in Ionic Liquids. *Chem. Rev.* **2014**, *114*, 1289–1326. [CrossRef] [PubMed]
14. Brennecke, J.F.; Gurkan, B.E. Ionic Liquids for CO_2 Capture and Emission Reduction. *J. Phys. Chem. Lett.* **2010**, *1*, 3459–3464. [CrossRef]
15. Olivier-Bourbigou, H.; Magna, L.; Morvan, D. Ionic Liquids and Catalysis: Recent Progress from Knowledge to Applications. *Appl. Catal. A Gen.* **2010**, *373*, 1–56. [CrossRef]
16. Zhang, X.; Zhang, X.; Dong, H.; Zhao, Z.; Zhang, S.; Huang, Y. Carbon Capture with Ionic Liquids: Overview and Progress. *Energy Environ. Sci.* **2012**, *5*, 6668–6681. [CrossRef]
17. Hasib-ur-Rahman, M.; Siaj, M.; Larachi, F. Ionic Liquids for CO_2 Capture-Development and Progress. *Chem. Eng. Process. Process Intensif.* **2010**, *49*, 313–322. [CrossRef]
18. Li, X.; Ding, S.; Zhang, J.; Wei, Z. Optimizing Microstructure of Polymer Composite Membranes by Tailoring Different Ionic Liquids to Accelerate CO2 Transport. *Int. J. Greenh. Gas Control.* **2020**, *101*, 103136. [CrossRef]
19. Sodeifian, G.; Raji, M.; Asghari, M.; Rezakazemi, M.; Dashti, A. Polyurethane-SAPO-34 Mixed Matrix Membrane for CO_2/CH_4 and CO_2/N_2 Separation. *Chin. J. Chem. Eng.* **2019**, *27*, 322–334. [CrossRef]
20. Wang, Y.; Nie, J.; Lu, C.; Wang, F.; Ma, C.; Chen, Z.; Yang, G. Imidazolium-Based Polymeric Ionic Liquids for Heterogeneous Catalytic Conversion of CO_2 into Cyclic Carbonates. *Microporous Mesoporous Mater.* **2020**, *292*, 109751. [CrossRef]
21. Baker, R.W.; Low, B.T. Gas Separation Membrane Materials: A Perspective. *Macromolecules* **2014**, *47*, 6999–7013. [CrossRef]
22. Favre, E. Membrane Processes and Postcombustion Carbon Dioxide Capture: Challenges and Prospects. *Chem. Eng. J.* **2011**, *171*, 782–793. [CrossRef]
23. Lian, S.; Song, C.; Liu, Q.; Duan, E.; Ren, H.; Kitamura, Y. Recent Advances in Ionic Liquids-Based Hybrid Processes for CO_2 Capture and Utilization. *J. Environ. Sci.* **2021**, *99*, 281–295. [CrossRef] [PubMed]
24. Zhou, Y.; Chang, M.; Zang, X.; Zheng, L.; Wang, Y.; Wu, L.; Han, X.; Chen, Y.; Yu, Y.; Zhang, Z. The polymeric ionic liquids/mesoporous alumina composites: Synthesis, characterization and CO_2 capture performance test. *Polym. Test.* **2020**, *81*, 106109. [CrossRef]
25. Bellina, F.; Bertoli, A.; Melai, B.; Scalesse, F.; Signori, F.; Chiappe, C. Synthesis and Properties of Glycerylimidazolium Based Ionic Liquids: A Promising Class of Task-Specific Ionic Liquids. *Green Chem.* **2009**, *11*, 622–662. [CrossRef]
26. Bernard, F.L.; dos Santos, L.M.; Schwab, M.B.; Polesso, B.B.; do Nascimento, J.F.; Einloft, S. Polyurethane-Based Poly(Ionic Liquid)s for CO_2 Removal from Natural Gas. *J. Appl. Polym. Sci.* **2019**, *136*, 4–11. [CrossRef]

27. da Luz, M.; Dias, G.; Zimmer, H.; Bernard, F.L.; do Nascimento, J.F.; Einloft, S. Poly(Ionic Liquid)s-Based Polyurethane Blends: Effect of Polyols Structure and ILs Counter Cations in CO_2 Sorption Performance of PILs Physical Blends. *Polym. Bull.* **2022**, *79*, 6123–6139. [CrossRef]
28. Morozova, S.M.; Lozinskaya, E.I.; Sardon, H.; Su, F.; Vlasov, P.S.; Vaudemont, R.; Vygodskii, Y.S.; Shaplov, A.S. Ionic Polyureas—A Novel Subclass of Poly(Ionic Liquid) s for CO_2 Capture. *Membranes* **2020**, *10*, 240. [CrossRef]
29. Morozova, S.M.; Shaplov, A.S.; Lozinskaya, E.I.; Mecerreyes, D.; Sardon, H.; Zulfiqar, S.; Suárez-García, F.; Vygodskii, Y.S. Ionic Polyurethanes as a New Family of Poly(Ionic Liquid)s for Efficient CO_2 Capture. *Macromolecules* **2017**, *50*, 2814–2824. [CrossRef]
30. Morozova, S.M.; Shaplov, A.S.; Lozinskaya, E.I.; Vlasov, P.S.; Sardon, H.; Mecerreyes, D.; Vygodskii, Y.S. Poly(Ionic Liquid)-Based Polyurethanes Having Imidazolium, Ammonium, Morpholinium or Pyrrolidinium Cations. *High Perform. Polym.* **2017**, *29*, 691–703. [CrossRef]
31. Dong, Y.; Holm, J.; Kärkkäinen, J.; Nowicki, J.; Lassi, U. Dissolution and Hydrolysis of Fibre Sludge Using Hydroxyalkylimidazolium Hydrogensulphate Ionic Liquids. *Biomass Bioenergy* **2014**, *70*, 461–467. [CrossRef]
32. Duan, N.; Sun, Z.; Ren, Y.; Liu, Z.; Liu, L.; Yan, F. Imidazolium-Based Ionic Polyurethanes with High Toughness, Tunable Healing Efficiency and Antibacterial Activities. *Polym. Chem.* **2020**, *11*, 867–875. [CrossRef]
33. Sonnenschein, M.F.; Lysenko, Z.; Brune, D.A.; Wendt, B.L.; Schrock, A.K. Enhancing Polyurethane Properties via Soft Segment Crystallization. *Polymer* **2005**, *46*, 10158–10166. [CrossRef]
34. Tsai, T.H.; Maes, A.M.; Vandiver, M.A.; Versek, C.; Seifert, S.; Tuominen, M.; Liberatore, M.W.; Herring, A.M.; Coughlin, E.B. Synthesis and Structure-Conductivity Relationship of Polystyrene-Block- Poly(Vinyl Benzyl Trimethylammonium) for Alkaline Anion Exchange Membrane Fuel Cells. *J. Polym. Sci. B Polym. Phys.* **2013**, *51*, 1751–1760. [CrossRef]
35. ASTM D822 Standard. Available online: https://industrialphysics.com/standards/astm-d822/ (accessed on 2 July 2024).
36. Barboza, E.M.; Delpech, M.C.; Garcia, M.E.F.; Pimenta, F.D. Avaliação Das Propriedades de Barreira de Membranas Obtidas a Partir de Dispersões Aquosas à Base de Poliuretanos e Argila. *Polimeros* **2014**, *24*, 94–100. [CrossRef]
37. Ferrari, H.Z.; Rodrigues, D.M.; Bernard, F.L.; dos Santos, L.M.; Le Roux, C.; Micoud, P.; Martin, F.; Einloft, S. A New Class of Fillers in Mixed Matrix Membranes: Use of Synthetic Silico-Metallic Mineral Particles (SSMMP) as a Highly Selective Component for CO_2/N_2 Separation. *Chem. Eng. J. Adv.* **2023**, *14*, 100488. [CrossRef]
38. Waheed, N.; Mushtaq, A.; Tabassum, S.; Gilani, M.A.; Ilyas, A.; Ashraf, F.; Jamal, Y.; Bilad, M.R.; Khan, A.U.; Khan, A.L. Mixed Matrix Membranes Based on Polysulfone and Rice Husk Extracted Silica for CO_2 Separation. *Sep. Purif. Technol.* **2016**, *170*, 122–129. [CrossRef]
39. Wu, H.; Thibault, J.; Kruczek, B. The Validity of the Time-Lag Method for the Characterization of Mixed-Matrix Membranes. *J. Memb. Sci.* **2021**, *618*, 118715. [CrossRef]
40. Jacoby, C.G. Síntese de Compostos Imidazol-Tiazolidina e Sua Aplicação como Organocatalisadores em Reações Aldólicas Estereosseletivas. Master's Thesis, The Federal University of Rio Grande do Sul, Porto Alegre, Brazil, 2016.
41. Vollas, A.; Chouliaras, T.; Deimede, V.; Ioannides, T. New Pyridinium Type Poly(Ionic Liquids) as Membranes for CO_2 Separation. *Polymers* **2018**, *10*, 912. [CrossRef]
42. Yu, G.; Man, Z.; Li, Q.; Li, N.; Wu, X.; Asumana, C.; Chen, X. New Crosslinked-Porous Poly-Ammonium Microparticles as CO_2 Adsorbents. *React. Funct. Polym.* **2013**, *73*, 1058–1064. [CrossRef]
43. Zhang, Z.; Gai, H.; Li, Q.; Feng, B.; Xiao, M.; Huang, T.; Song, H. Effect Anions on the Hydrogenation of Nitrobenzene over N-Rich Poly(Ionic Liquid) Supported Pd Catalyst. *Chem. Eng. J.* **2022**, *429*, 132224. [CrossRef]
44. Chiappe, C.; Pomelli, C.S.; Rajamani, S. Influence of Structural Variations in Cationic and Anionic Moieties on the Polarity of Ionic Liquids. *J. Phys. Chem. B* **2011**, *115*, 9653–9661. [CrossRef] [PubMed]
45. Guo, J.; Zhao, M.; Ti, Y.; Wang, B. Study on Structure and Performance of Polycarbonate Urethane Synthesized via Different Copolymerization Methods. *J. Mater. Sci.* **2007**, *42*, 5508–5515. [CrossRef]
46. Rogulska, M. Polycarbonate-Based Thermoplastic Polyurethane Elastomers Modified by DMPA. *Polym. Bull.* **2019**, *76*, 4719–4733. [CrossRef]
47. Cakić, S.M.; Špírková, M.; Ristić, I.S.; B-Simendić, J.K.; M-Cincović, M.; Poręba, R. The Waterborne Polyurethane Dispersions Based on Polycarbonate Diol: Effect of Ionic Content. *Mater. Chem. Phys.* **2013**, *138*, 277–285. [CrossRef]
48. Zhang, Y.; Sunarso, J.; Liu, S.; Wang, R. Current Status and Development of Membranes for CO2/CH4 Separation: A Review. *Int. J. Greenh. Gas Control.* **2013**, *12*, 84–107. [CrossRef]
49. Yuan, J.; Mecerreyes, D.; Antonietti, M. Poly(Ionic Liquid)s: An Update. *Prog. Polym. Sci.* **2013**, *38*, 1009–1036. [CrossRef]
50. Zhang, M.; Hemp, S.T.; Zhang, M.; Allen, M.H.; Carmean, R.N.; Moore, R.B.; Long, T.E. Water-Dispersible Cationic Polyurethanes Containing Pendant Trialkylphosphoniums. *Polym. Chem.* **2014**, *5*, 3795–3803. [CrossRef]
51. Behera, P.K.; Usha, K.M.; Guchhait, P.K.; Jehnichen, D.; Das, A.; Voit, B.; Singha, N.K. A Novel Ionomeric Polyurethane Elastomer Based on Ionic Liquid as Crosslinker. *RSC Adv.* **2016**, *6*, 99404–99413. [CrossRef]
52. Vila, J.; Varela, L.M.; Cabeza, O. Cation and Anion Sizes Influence in the Temperature Dependence of the Electrical Conductivity in Nine Imidazolium Based Ionic Liquids. *Electrochim. Acta* **2007**, *52*, 7413–7417. [CrossRef]
53. Zulfiqar, S.; Sarwar, M.I.; Mecerreyes, D. Polymeric Ionic Liquids for CO_2 Capture and Separation: Potential, Progress and Challenges. *Polym. Chem.* **2015**, *6*, 6435–6451. [CrossRef]
54. Raza, A.; Farrukh, S.; Hussain, A.; Khan, I.; Othman, M.H.D.; Ahsan, M. Performance Analysis of Blended Membranes of Cellulose Acetate with Variable Degree of Acetylation for CO_2/CH_4 Separation. *Membranes* **2021**, *11*, 245. [CrossRef]

55. Mubashir, M.; Yeong, Y.F.; Lau, K.K.; Chew, T.L.; Norwahyu, J. Efficient CO_2/N_2 and CO_2/CH_4 Separation Using NH_2-MIL-53(Al)/Cellulose Acetate (CA) Mixed Matrix Membranes. *Sep. Purif. Technol.* **2018**, *199*, 140–151. [CrossRef]
56. Farrokhara, M.; Dorosti, F. New High Permeable Polysulfone/Ionic Liquid Membrane for Gas Separation. *Chin. J. Chem. Eng.* **2020**, *28*, 2301–2311. [CrossRef]
57. Sajjan, P.; Nayak, V.; Padaki, M.; Zadorozhnyy, V.Y.; Klyamkin, S.N.; Konik, P.A. Fabrication of Cellulose Acetate Film through Blending Technique with Palladium Acetate for Hydrogen Gas Separation. *Energy Fuels* **2020**, *34*, 11699–11707. [CrossRef]
58. Akbarzadeh, E.; Shockravi, A.; Vatanpour, V. High Performance Compatible Thiazole-Based Polymeric Blend Cellulose Acetate Membrane as Selective CO_2 Absorbent and Molecular Sieve. *Carbohydr. Polym.* **2021**, *252*, 117215. [CrossRef]
59. Bara, J.E.; Lessmann, S.; Gabriel, C.J.; Hatakeyama, E.S.; Noble, R.D.; Gin, D.L. Synthesis and Performance of Polymerizable Room-Temperature Ionic Liquids as Gas Separation Membranes. *Ind. Eng. Chem. Res.* **2007**, *46*, 5397–5404. [CrossRef]
60. Bara, J.E.; Gabriel, C.J.; Hatakeyama, E.S.; Carlisle, T.K.; Lessmann, S.; Noble, R.D.; Gin, D.L. Improving CO2 Selectivity in Polymerized Room-Temperature Ionic Liquid Gas Separation Membranes through Incorporation of Polar Substituents. *J. Memb. Sci.* **2008**, *321*, 3–7. [CrossRef]
61. Horne, W.J.; Andrews, M.A.; Shannon, M.S.; Terrill, K.L.; Moon, J.D.; Hayward, S.S.; Bara, J.E. Effect of Branched and Cycloalkyl Functionalities on CO_2 Separation Performance of Poly(IL) Membranes. *Sep. Purif. Technol.* **2015**, *155*, 89–95. [CrossRef]
62. Shaligram, S.V.; Rewar, A.S.; Wadgaonkar, P.P.; Kharul, U.K. Incorporation of Rigid Polyaromatic Groups in Polybenzimidazole-Based Polymeric Ionic Liquids: Assertive Effects on Gas Permeation Properties. *Polymer* **2016**, *93*, 30–36. [CrossRef]
63. Fang, W.; Luo, Z.; Jiang, J. CO_2 Capture in Poly(Ionic Liquid) Membranes: Atomistic Insight into the Role of Anions. *Phys. Chem. Chem. Phys.* **2013**, *15*, 651–658. [CrossRef]
64. Robeson, L.M. The Upper Bound Revisited. *J. Memb. Sci.* **2008**, *320*, 390–400. [CrossRef]
65. Robeson, L.M. Correlation of Separation Factor versus Permeability for Polymeric Membranes. *J. Membr. Sci.* **1991**, *62*, 165–185. [CrossRef]
66. Zhang, M.; Semiat, R.; He, X. Recent Advances in Poly(Ionic Liquids) Membranes for CO_2 Separation. *Sep. Purif. Technol.* **2022**, *299*, 121784. [CrossRef]